

Anode Material Synthesized from Red Phosphorus and Germanium Nanowires for Lithium-Ion and Sodium-Ion Batteries

Tatiana Kulova¹, Dmitri Gryzlov¹, Alexander Skundin¹, Iliya Gavrilin^{1,2}, Yulia Kudryashova¹, Nicolai Pokryshkin³

¹ Frumkin Institute of Physical Chemistry and Electrochemistry of the RAS, 31-4 Leninskii ave., 119071 Moscow, Russia

² National Research University of Electronic Technology (MIET), Bld. 1, Shokin Square, Zelenograd, 124498, Moscow Russia

³ National Research Nuclear University (MEPHI), 31, Kashirskoe ave., 115409, Moscow Russia

*E-mail: askundin@mail.ru

Received: 26 August 2021 / Accepted: 28 September 2021 / Published: 10 November 2021

Germanium phosphide (GeP) is synthesized by red phosphorus evaporation-condensation on the surface of germanium nanowires pre-grown on a titanium substrate. The synthesized GeP was found to be capable of reversibly inserting lithium and sodium. The effective diffusion coefficients of lithium and sodium in germanium phosphide are distinguished by 2 orders of magnitude and amounted to 10^{-12} and 10^{-14} cm²/s, respectively.

Keywords: germanium, germanium phosphide, lithium and sodium diffusion coefficient, lithium-ion battery, sodium-ion battery.

1. INTRODUCTION

Modern commercial lithium-ion batteries have an energy density of about 250 Wh/kg [1]. The developed sodium-ion batteries are inferior to lithium-ion batteries in terms of energy density but are considered more environmentally friendly and economical. A further increase in the energy characteristics of lithium-ion and sodium-ion batteries depends on the possibility of synthesizing more energy-intensive functional cathode and anode materials. The most popular anode material for lithium-ion batteries is graphite, with a theoretical specific capacity of 372 mAh/g. The theoretical capacity of hard carbon when sodium is inserted is about 300 mAh/g. At the same time, there are a number of materials whose specific insertion capacity for lithium and sodium is significantly higher than that of

carbon-based materials. Recently, much attention has been paid to germanium, which is capable of forming various compounds with lithium and sodium up to $\text{Li}_{22}\text{Ge}_5$, and Na_3Ge [2]. The theoretical specific capacity of germanium in the formation of these compounds is 1624 and 1107 mAh/g, respectively.

Germanium can form compounds with phosphorus of the composition GeP , GeP_3 , and GeP_5 , and such compounds can reversibly insert lithium [3–7] and sodium [8–17]. The main problem with high-capacity inserting materials is the low cyclic stability associated with the degradation of the functional material. The theoretical specific capacity of GeP upon reversible insertion of lithium and sodium can reach 1914 and 1552 mAh/g, respectively.

This paper proposes a new method for the synthesis of germanium phosphide, which is stable under the reversible insertion of lithium and sodium.

2. EXPERIMENTAL

2.1 Preparation of composite samples.

The electrodes investigated were based on titanium plates with germanium nanowires with an average diameter of about 30 nm and a length of up to 0.5 μm . The procedure for obtaining germanium nanowires is described in detail in [18, 19]. Before the deposition of germanium nanowires, the surface of the plates was cleaned in an aqueous solution containing H_2O_2 and NH_4OH and activated in a mixture of hydrofluoric and nitric acids. Arrays of spherical indium nanoparticles were then formed on this surface by vacuum-thermal evaporation and served subsequently as seeds (crystallization centers) for the growth of germanium nanowires. Germanium nanowires were produced by cathodic deposition from an electrolyte obtained by dissolving GeO_2 in a mixture of aqueous solutions of potassium sulfate and succinic acid. The deposition was carried out at a current density of 2 mA/cm^2 . The mass of the obtained germanium nanowires was about 330 $\mu\text{g}/\text{cm}^2$. The samples prepared in this way were washed and dried in an argon flow. Then these samples were transferred into a glove box with an argon atmosphere (Spektroskopicheskie Sistemy, Russia. The water and oxygen content in the box did not exceed 1 ppm) and placed in sealed stainless steel ampoules. Red phosphorus was added to the same ampoules in stoichiometric excess to the amount of germanium. These ampoules were then placed in a tube furnace, heated to 650 °C kept at this temperature for 30 min, and then cooled naturally. The phosphorus first sublimated and then condensed on the surface of the germanium nanowires to form germanium phosphides.

2.2 Characterization of the composites.

The synthesized composite samples were characterized using X-ray phase analysis, scanning electron microscopy, and Raman spectroscopy.

The phase composition of the prepared samples was studied using the X-ray diffraction (XRD) patterns and Raman spectroscopy.

X-ray diffraction (XRD) patterns of the prepared samples were collected using an x-ray diffractometer Radian DR-02 equipped with a Cu-K α X-ray source. Backscattered Raman spectra were measured under excitation with focused laser radiation using an MR350 micro-Raman spectrometer. In our experiments, we used He-Ne laser (wavelength 633 nm, maximal power 6 mW, minimal spot radius 8 μ m).

The morphology of the samples was studied by scanning electron microscopy (SEM) using Carl Zeiss Supra 40-30-87 microscope.

2.3 Electrochemical research

Electrochemical characteristics of the synthesized germanium phosphide samples were investigated by cyclic voltammetry, chronoamperometry, and electrochemical impedance spectroscopy. The electrochemical cells contained three electrodes: the working electrode, a synthesized germanium phosphide sample, the auxiliary electrode, and the reference electrode. The auxiliary and reference electrodes were made of lithium (in the lithium insertion/extraction study) or sodium (in the sodium insertion/extraction study), rolled onto a substrate of nickel foil. All electrodes were separated by a polypropylene separator (NPO "Ufim," Russia). The electrolyte used was 1 M LiClO $_4$ in a mixture of propylene carbonate (PC)–dimethoxyethane (7: 3) or 1 M NaClO $_4$ in a mixture of PC–ethylene carbonate (1: 1). The water content of the electrolytes determined by Fischer coulometric titration (917 Coulometer, Metrohm) did not exceed 15 ppm. All cell assembly and electrolyte filling operations were carried out in the already mentioned glove box with an argon atmosphere.

Electrochemical cells were galvanostatically cycled using an AZRIVK-50-10V galvanostat (JSC "Buster", Russia). The current densities during galvanostatic cycling were 800, 1600, 3200, 6400, 12800 mA/g for lithium insertion/extraction and 30, 60, 120, 240, 480 mA/g for sodium insertion/extraction. The cycling potential range was from 0.01 to 3.0 V. Cyclic voltammetry curves of the test samples were recorded using a P-20X potentiostat (ELINS STC JSC, Russia). The potential scan rates were 0.1, 0.2, 0.4, 0.8, and 1.6 mV/s. The electrochemical impedance spectra were registered using frequency analyzer "Solartron" (Model 1255 HF) and electrochemical interface "Solartron" (Model 1286) with voltage amplitude 10 mV and frequency range from 100 kHz to 100 mHz at a potential of 250–260 mV. The resulting impedance spectra were analysed using ZView software.

3. RESULTS AND DISCUSSION

3.1 Morphological and physicochemical studies

Fig.1 shows scanning electron microscope images of the synthesized germanium phosphide sample.

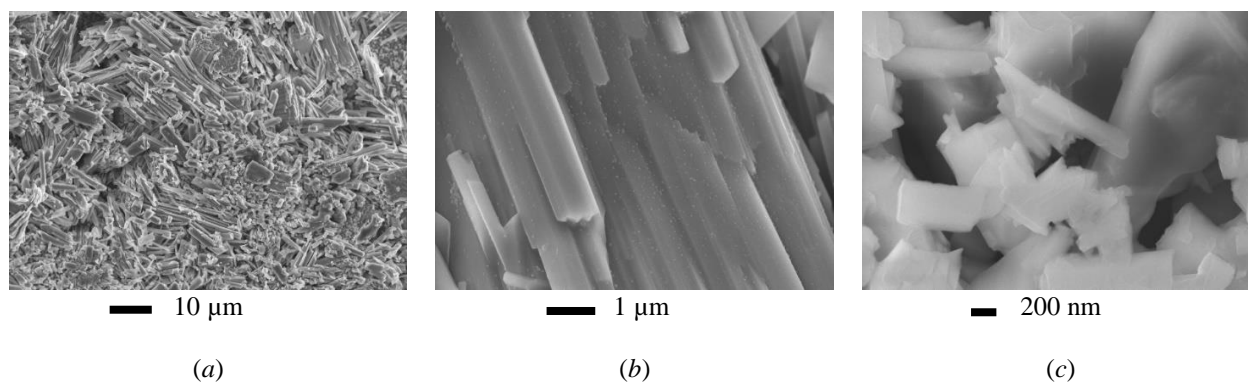


Figure 1. Scanning electron microscope images of the synthesized germanium phosphide sample at different magnifications

As it can be seen, the high-temperature treatment in a phosphorus vapor atmosphere turns the original germanium nanowires into nanorods with a diameter between 250 and 500 nm and a length between 0.2 and 10 μm . With sufficiently high magnification, the homogeneous morphology of the resulting composites is clearly visible. Electron dispersive analysis detects germanium, phosphorus, titanium, oxygen, and carbon in such samples.

Fig. 2 shows the results of the X-ray phase analysis of the original composite sample. The peaks from the titanium substrate are clearly visible here, as well as a large set of peaks related to germanium phosphide GeP. The XRD patterns agree by and large with literature data [3, 4, 11]. Some shift of these peaks relative to the COD (Crystallography Open Database) data indicates that the lattice of this phase is somewhat stretched.

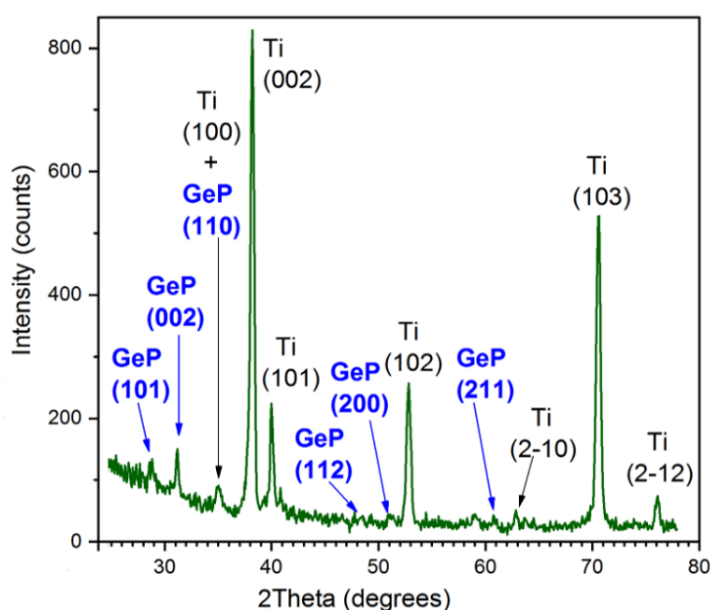


Figure 2. XRD patterns of GeP sample on titanium substrate

The Raman light scattering spectrum (Fig. 3) shows several peaks in the region of 300–500 cm^{-1} and an intense peak in the region of 950–1100 cm^{-1} . The peaks in the 300–500 cm^{-1} region can be attributed to the compounds of germanium with phosphorus. The peak at 950–1100 cm^{-1} corresponds to compounds of titanium with phosphorus, for example, γ -TiP [20].

Thus, the results of X-ray diffraction and Raman spectroscopy indicate the formation of GeP germanium phosphide.

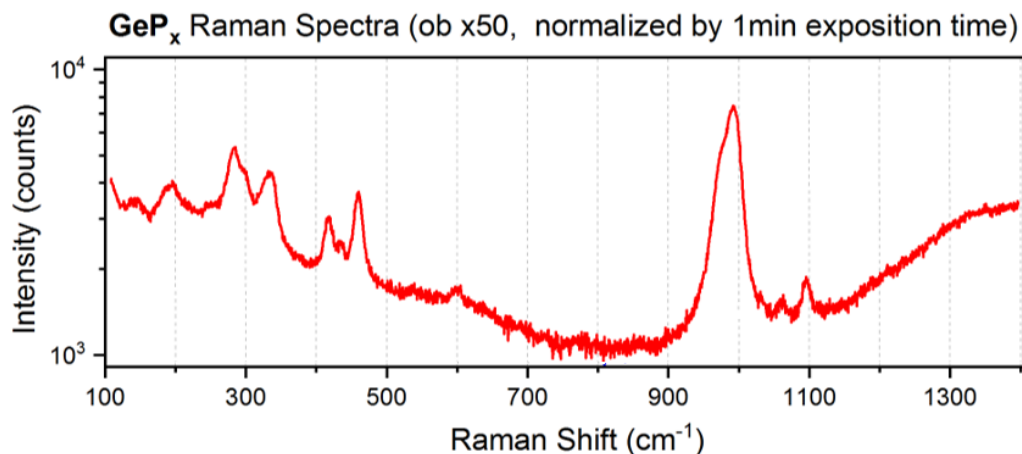


Figure 3. Raman light scattering spectra of a synthesized germanium phosphide sample

3.2 Electrochemical measurements. Insertion/extraction of lithium to/from GeP.

The cyclic voltammetry (CV) curves of the synthesized GeP sample during lithium insertion/extraction, obtained at various potential scan rates, are shown in Fig. 4a.

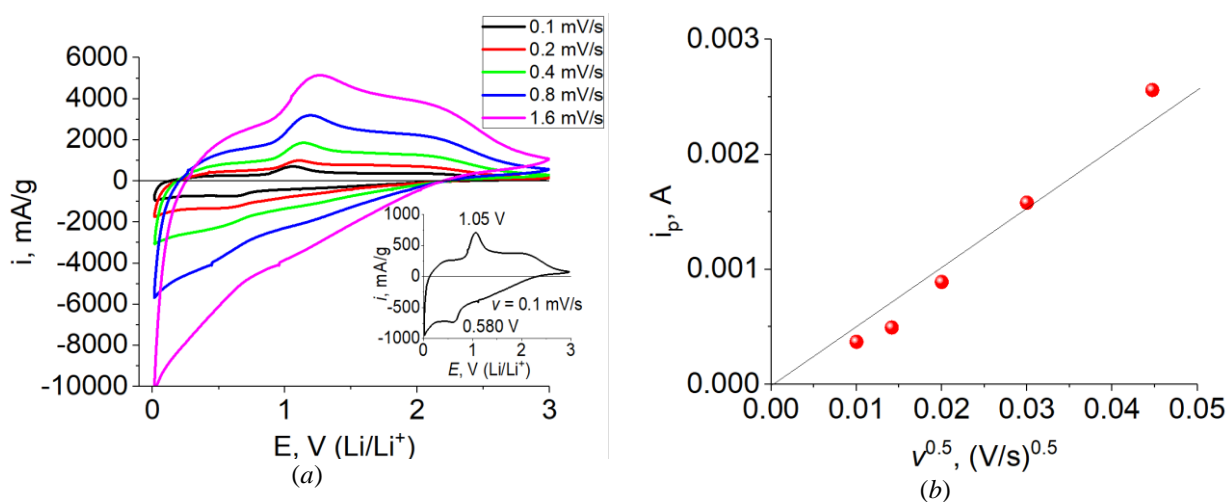


Figure 4. Cyclic voltammograms of the GeP sample at different potential scan rates (a) and the dependence of the anodic current peak on the square root of the potential scan rate (b)

The CV cathode branch reflects the process of lithium insertion into GeP, while the anodic branch reflects the process of lithium extraction from the lithiated GeP. The inset of Fig. 4a shows the GeP CV scaled up along the ordinate at a potential scan rate of 0.1 mV/s. As can be seen from the Figure, clear cathode and anode peaks are recorded on the CVs, reflecting the reversible nature of lithium insertion in GeP. Similar CV-behavior of GeP-based electrodes was reported in [3, 4]. An increased potential scan rate leads to an increase in cathode and anode currents, and a shift in current peaks in the positive and negative directions for the anode and cathode current peaks, respectively. Fig. 4b shows the dependence of the maximum anode current recorded in the potential region of around 1 V on the square root of the potential scan rate. The dependence of the current on the potential scan rate is linear and passes through the origin of coordinates, indicating the diffusive nature of lithium insertion into germanium phosphide.

The galvanostatic curves shown in Fig. 5 demonstrate the change in the shape of the charge-discharge curves when the current density increases.

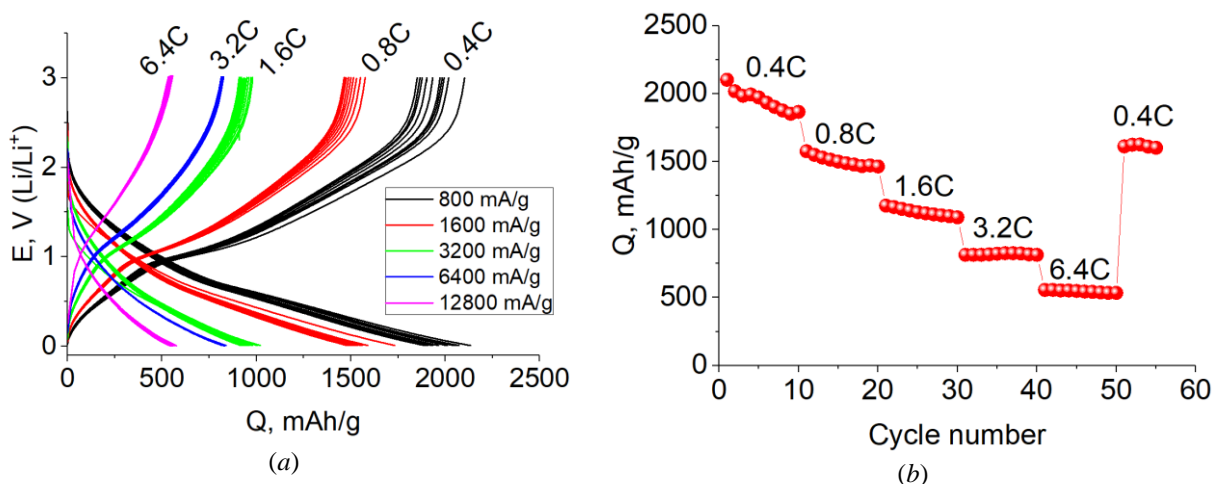


Figure 5. Charge-discharge curves of the GeP sample upon lithium insertion at various current densities (a) and dependence of the discharge capacity on the current density (b)

The current density of 800 mA/g approximately corresponded to the 0.4 C rate. At this current density, the discharge (anode) capacity was close to the theoretical discharge capacity, which is 1915 mAh/g. During cycling, a slight decrease in the discharge capacity was recorded at the initial cycles; however, with further cycling, no degradation was observed. Some excess of the discharge capacity compared to the theoretical specific capacity can be due to the reversible insertion of lithium into titanium monophosphide formed by the interaction of the titanium substrate with red phosphorus vapor. This fact is confirmed by cyclic voltammetry of titanium monophosphide (Fig. 6).

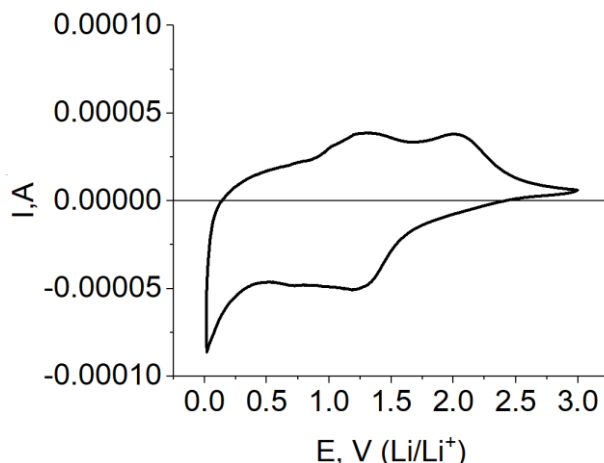


Figure 6. Cyclic voltammograms on a titanium substrate treated in red phosphorus vapor. Potential scan rate 0.1 mV/s

3.3 Insertion/extraction of sodium in GeP.

Cyclic voltammograms of sodium insertion/extraction into/from GeP are shown in Fig. 7a. The CVs form differs from that in the insertion/extraction of lithium. The similar distinction between CV curves for sodium and lithium insertion/extraction was noted in [11] but in the present work this distinction is expressed more clearly.

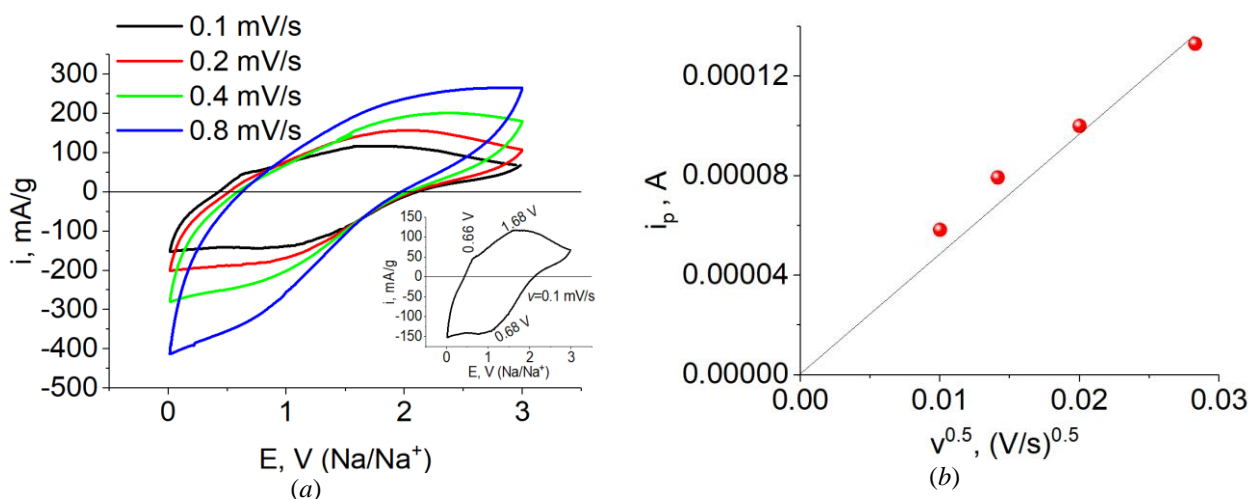


Figure 7. Cyclic voltammograms (a) and dependence of the peak current on the square root of the potential scan rate (b) for the sodium insertion/extraction into/from GeP

At a potential scan rate of 0.1 mV/s, the CV recorded peaks reflecting the process of sodium insertion and extraction, which is clearly seen in the inset in Fig. 7a. With the potential scan rate increase, the reversible peaks become blurred. The dependence of the peak current on the square root of the

potential scan rate (Fig.7b) is linear and passes through the origin of coordinates, which indicates the diffusive nature of the process of sodium insertion/extraction into GeP, as it does for lithium. It is worth noting that the cyclic voltammetry of the titanium substrate treated with phosphorus vapor showed the absence of the reaction of reversible sodium insertion into titanium monophosphide.

Charge-discharge curves and the dependence of the discharge capacity of GeP on the current density during the insertion/extraction of sodium are shown in Fig. 8. As can be seen from Fig. 8, at a sufficiently low current density of 30 mA/g (0.019 C), two plateaus corresponding to sodium extraction from GeP are recorded on the anode branch of the charge-discharge curve. At this current density, the discharge capacity was about 1300 mA/g. An increase in the current density leads to a decrease in the discharge capacity and disappearance of clear plateaus on the charge-discharge curve. At a current density of 480 mA/g (0.3C), the discharge capacity did not exceed 130 mAh/g.

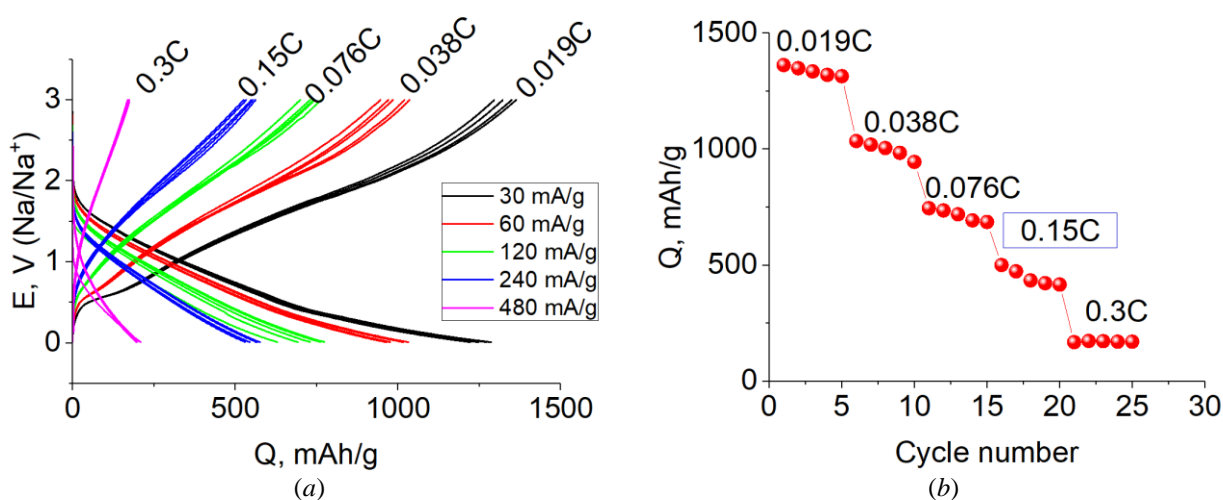


Figure 8. Charge-discharge curves (a) and dependence of the GeP discharge specific capacity upon the insertion of sodium at various current densities (b).

3.4 Estimation of the effective diffusion coefficient of lithium and sodium in GeP based on cyclic voltammograms.

Using the Randles-Ševčík equation [21, 22], one can estimate with some approximation the effective diffusion coefficient of lithium and sodium in GeP.

$$i_p = 0.4463nFAc \frac{(nFvD)^{1/2}}{(RT)^{1/2}} \quad (1)$$

Here i_p is a peak current (A), v is the potential scan rate (V/s), A is the true surface area (cm^2), c is the concentration of lithium ions (mol/cm^3), R - universal gas constant (J/Kmol), F is the Faraday number ($\text{A}\cdot\text{s}/\text{mole}$).

Taking into account the non-Nernst dependence of the potential of the insertion compound on the concentration of the alkali metal ion, equation (1) is transformed into equation (2)

$$D = \frac{i_p^2}{0.4463^2 n^2 F^2 A^2 c v} \frac{dE}{dc} \quad (2).$$

The true surface area S of the GeP sample was estimated by the formula:

$$S = \frac{2}{r\rho}, \quad (3)$$

where r is the radius of the GeP nanorod, ρ is the GeP density (4 g/cm^3). The true GeP surface area by the order was $10,000 \text{ cm}^2/\text{g}$ or 5 cm^2 .

The ratio $i_p/v^{0.5}$ calculated from Fig. 4b was $0.064 \text{ A}\cdot\text{V}^{0.5}/\text{s}^{0.5}$. The concentration of lithium in GeP is related to the passed charge Q by the obvious relation

$$c = Q\rho / F \quad (4)$$

At a potential of 1.05 V, the lithium concentration was 0.233 mol/cm^3 , and the derivative dE/dc defined from the graph shown in Fig. 9a, was about $3.3 \text{ V}\cdot\text{cm}^3/\text{mol}$.

The ratio $i_p/v^{0.5}$ calculated from Fig. 8b in the case of sodium insertion/extraction was $0.004 \text{ A}\cdot\text{V}^{0.5}/\text{s}^{0.5}$. The sodium concentration in GeP was 0.101 mol/cm^3 . The derivative dE/dc calculated from the graph shown in Fig. 9b, at a potential of 1.68 V was about $8.6 \text{ V}\cdot\text{cm}^3/\text{mol}$.

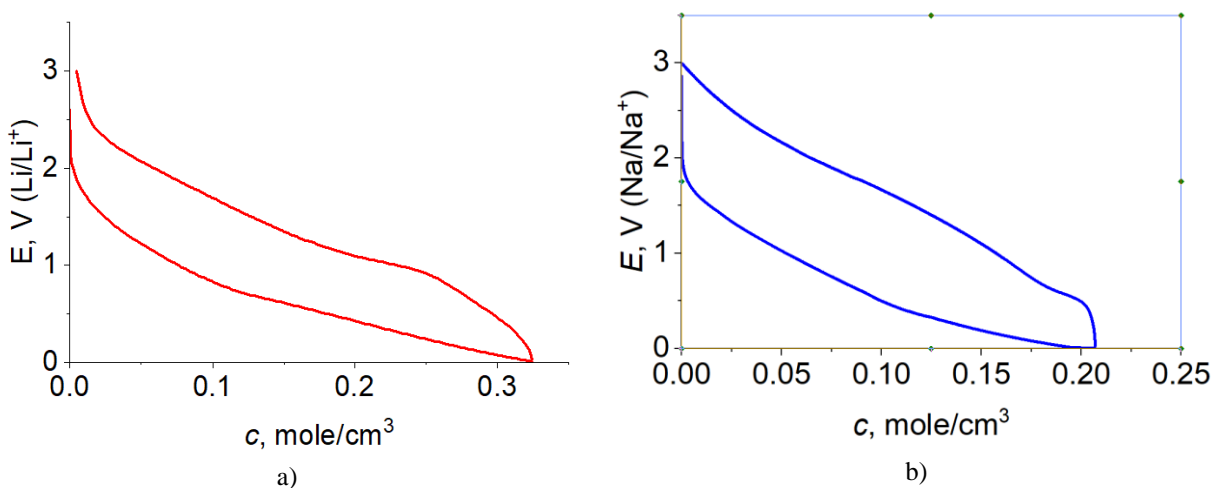


Figure 9. Dependence of the GeP potential on the concentration of inserted lithium (a) and sodium (b)

The effective diffusion coefficients of lithium and sodium in GeP were about $1.2 \cdot 10^{-12} \text{ cm}^2/\text{s}$ and $3 \cdot 10^{-14} \text{ cm}^2/\text{s}$, respectively. Noteworthy is that Refs [3] and [11] present no quantitative information on lithium and sodium diffusion coefficients in GeP.

3,5 Comparison of the GeP electrochemical behavior under reversible insertion of lithium and sodium.

Fig. 10 shows the dependences of the GeP discharge capacity on the current density during the insertion of lithium and sodium in logarithmic coordinates.

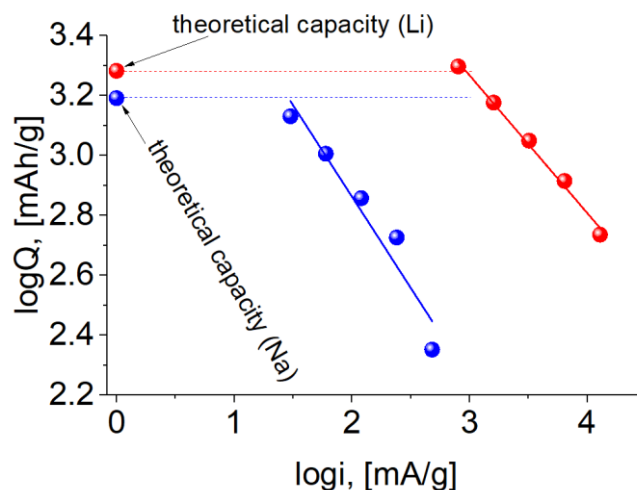


Figure 10. Logarithmic dependence of the GeP discharge capacity on the current density upon the insertion/extraction of lithium and sodium

In a certain range of current densities, the dependence of the capacity on the current density is described by the Peukert equation [23]:

$$Q_d = i^b t \text{ or } \log Q_d = a + b \log i, \quad (5)$$

where Q_d is the discharge capacity, a is the logarithm of the discharge capacity at an infinitesimal current, b is the slope of the dependence $\log Q = f(\log i)$, which characterizes the degree of change in the discharge capacity with a change in the current density. Upon the insertion/extraction of lithium, the slope b was -0.46 , while upon the insertion/extraction of sodium, the slope b was -0.61 . (In this respect the behavior of GeP differs from that of germanium-carbon composite studied recently [24]).

The dependences $\log Q = f(\log i)$ show that when lithium is inserted at current densities of about 800 mA/g (0.4 C), the discharge capacity is practically equal to the theoretical value, while with sodium insertion, the theoretical capacity can only be achieved at extremely low current densities 30 mA/g (0.019 C). The greater slope of the dependence $\log Q = f(\log i)$ upon interaction with sodium indicates a greater difficulty of sodium insertion compared to that of lithium.

It is interesting to compare the performance of material suggested in the present work with available literature data. Such a comparison is presented in the Table 1. One can see that the material of the present work demonstrates much higher specific capacity for lithium insertion than the literature counterparts [3, 4]. In the process of sodium insertion the preference of novel material is revealed at low and modest C-rates.

Table 1. The insertion performances of GeP-based materials

| Current, A/g | C-rate | Specific capacity, mAh/g | Reference |
|-------------------|--------|--------------------------|------------------|
| Lithium insertion | | | |
| 0.5 | 0.25 | 1300 | [3] |
| 5 | 2.5 | 800 | [3] |
| 0.1 | 0.05 | 1500 | [4] |
| 0.8 | 0.4 | 2000 | The present work |
| 6.4 | 3.2 | 800 | The present work |
| 12.8 | 6.4 | 550 | The present work |
| Sodium insertion | | | |
| 0.1 | 0.067 | 400 | [11] |
| 1 | 0.67 | 260 | [11] |
| 4 | 2.7 | 100 | [11] |
| 0.03 | 0.02 | 1300 | The present work |
| 0.225 | 0.15 | 400 | The present work |
| 0.45 | 0.3 | 200 | The present work |

3.6 Impedance studies of germanium phosphide upon the insertion of lithium and sodium.

Fig. 11 shows the results of impedance measurements of the GeP sample upon the insertion of lithium and sodium and the corresponding equivalent circuit.

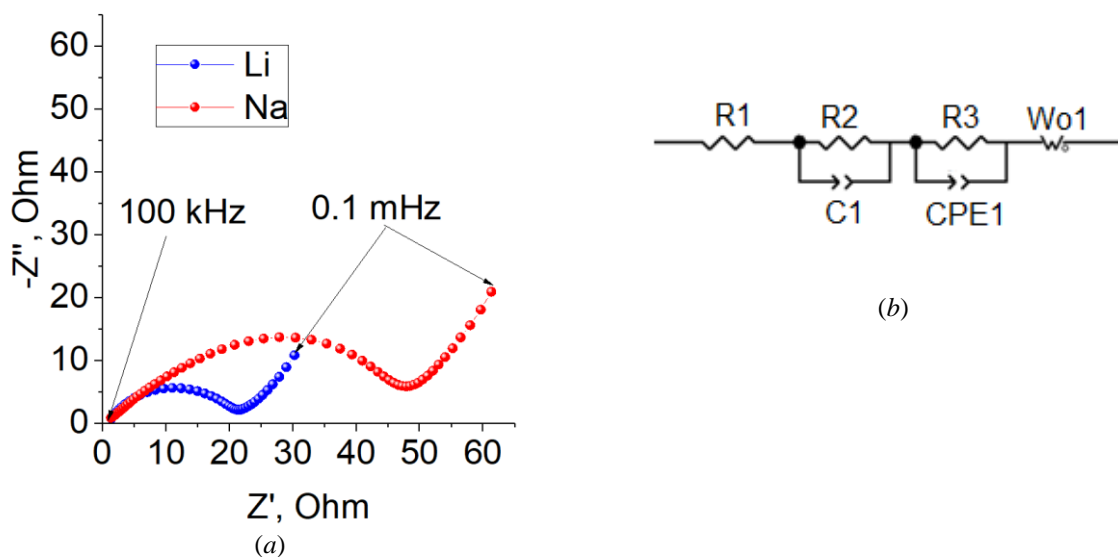


Figure 11. Impedance diagrams of GeP upon the insertion of lithium (the blue curve) and sodium (the red curve) (a) and equivalent circuit (b). Measurement potential 265 mV

The equivalent circuit includes electrolyte resistance (R1), passive film resistance (R2), passive film capacitance (C1), charge transfer resistance (R3), constant phase shift element (CPE2) characterizing the capacity of the electric double layer, and Warburg element (Wo1) characterizing the solid phase diffusion of the alkali metal ion (lithium or sodium). This impedance circuit has previously been used by the authors to investigate the insertion of lithium into germanium nanowires [19].

Table 2 shows the experimental values of the equivalent circuit parameters for the spectra shown in Figure 11.

Table 2. Experimental values of the equivalent circuit parameters

| | R1, Ohm | R2, Ohm | C1, F | R3, Ohm | CPE-T, F | CPE-P | W _R , Ohm/s ^{0.5} | W _T , Ohm/s ^{0.5} | W _P |
|--------|---------|---------|-----------------------|---------|----------------------|-------|---------------------------------------|---------------------------------------|----------------|
| GeP+Li | 1.7 | 3.6 | 1.02·10 ⁻⁵ | 14 | 0.001 | 0.85 | 25.47 | 4.6619 | 0.44 |
| GeP+Na | 1.4 | 3.2 | 2.6·10 ⁻⁵ | 41 | 4.8·10 ⁻⁵ | 0.73 | 48 | 1.386 | 0.44 |

The capacitance of the double layer at the interface (C_{dl}) was calculated using the equation:

$$C_{dl} = T^{1/P} R_{ct}^{(1/P-1)} \quad (6),$$

where T is (CPE-T) and P is (CPE-P)

The values of the Warburg constant were determined by the equation:

$$W = W_R / (2 * W_T)^{W_P} \quad (7)$$

The calculated values of the parameters of the equivalent circuit for the impedance spectra of the germanium phosphide-based electrode with respect to the true GeP surface area are shown in Table 3.

Table 3. Calculated values of the equivalent circuit parameters

| | R1, Ohm | R2, Ohm·cm ² | C1, F/cm ² | R3, Ohm·cm ² | C _{dl} , F/cm ² | W _o , Ohm/s ^{0.5} |
|--------|---------|-------------------------|-----------------------|-------------------------|-------------------------------------|---------------------------------------|
| GeP+Li | 1.7 | 18.0 | 2.1·10 ⁻⁶ | 70.0 | 1.3·10 ⁻⁶ | 9.6 |
| GeP+Na | 1.4 | 16.0 | 5.3·10 ⁻⁶ | 205.0 | 4.8·10 ⁻⁶ | 30.6 |

As can be seen from the Table 3, upon the insertion of lithium, the capacitance of the GeP double layer in lithium-containing and sodium-containing electrolytes was almost identical and amounted to 1.3·10⁻⁶ F/cm² and 4.8·10⁻⁵ F/cm², respectively. The solid electrolyte film resistance and its capacitance also had little difference in lithium-containing and sodium-containing electrolytes. The charge transfer resistance was found to be significantly higher with sodium insertion. The Warburg constant upon the insertion of lithium and sodium was 9.6 and 24 Ohm/s^{0.5}, respectively.

The solid-phase diffusion coefficients for an alkali metal ion using the Warburg constant can be calculated using the formula:

$$D = 0.5 \left(\frac{dE}{dc} \frac{1}{nFAW} \right)^2 \quad (8),$$

where F is the Faraday number, A is the true surface area, W is the Warburg constant, dE/dc is the slope of the potential-concentration dependence, taking into account the non-Nernst dependence of the potential on concentration.

For lithium extraction, the derivative dE/dc was $11.9 \text{ V}\cdot\text{cm}^3/\text{mol}$, and the calculated effective diffusion coefficient of lithium in GeP was $3.3\cdot 10^{-12} \text{ cm}^2/\text{s}$. For sodium extraction, the derivative dE/dc was $5.34 \text{ V}\cdot\text{cm}^3/\text{mol}$ and the calculated effective diffusion coefficient of sodium in GeP was $6.5\cdot 10^{-14} \text{ cm}^2/\text{s}$. Thus, the values of lithium and sodium diffusion coefficients calculated from CVs and impedance spectroscopy data coincide within orders of magnitude. Note, however, that the diffusion coefficients determined in this paper from cyclic voltammetric and impedance measurements refer to different potential values.

4. CONCLUSION

In this work, we prepared and studied electrodes based on germanium phosphide GeP nanorods. First, germanium nanowires with a diameter of about 30 nm were galvanically deposited on titanium substrates. Then, these nanowires were treated with red phosphorus vapor (evaporation-condensation method) to form GeP nanorods with a diameter of about 300 nm. The composition of the nanorods was determined from a combination of X-ray diffraction analysis (XRD) and Raman spectroscopy. The resulting material is capable of reversible insertion of lithium and sodium ions from the respective electrolytes and can be used in the negative electrodes of lithium-ion and sodium-ion batteries. The reversible capacity with lithium insertion is about 1900 and about 500 mAh/g at 0.4 C and 6.4 C rates. The specific capacity is considerably lower with sodium insertion: about 1300 mAh/g at a rate of 0.019 C and about 130 mAh/g at a rate of 0.3 C. This difference is related, in particular, to the difference in the effective diffusion coefficients of lithium and sodium, which are of the order of 10^{-12} and $10^{-14} \text{ cm}^2/\text{s}$, respectively.

FUNDING

The work is supported by the Russian Science Foundation (project no. 21-13-00160).

CONFLICT OF INTERESTS

The authors declare no conflicts of interest.

References

1. Vladimir S. Bagotsky, Alexander M. Skundin, Yuriy M. Volkovich. *Electrochemical Power Sources: Batteries, Fuel Cells, and Supercapacitors*. Wiley ISBN: 978-1-118-46023-8, 400 pages.
2. S. Wu, C. Han, J. Iocozzia, M. Lu, R. Ge, R. Xu, and Z. Lin, *Angew. Chem. Int. Ed.*, 55 (2016) 7898.
3. W. Li, X. Li, J. Yu, J. Liao, B. Zhao, L. Huang, A. Abdelhafiz, H. Zhang, J.-H. Wang, Z. Guo, and M. Liu, *Nano Energy*, 61 (2019) 594.
4. H. Shen, Y. Huang, Y. Chang, R. Hao, Z. Ma, K. Wu, P. Du, B. Guo, Y. Lyu, P. Wang, H. Yang, Q.

- Li, H.T. Wang, Z. Liu, and A.Nie, *ACS Appl. Mater. Interfaces*, 12 (2020) 17466
5. Y. Yan, J. Ruan, H. Xu, Y. Xu, Y. Pang, J. Yang, and S. Zheng, *ACS Appl. Mater. Interfaces*, 12 (2020) 21579.
 6. J. He, Y. Wei, L. Hu, H. Li, and T. Zhai, *Front. Chem.*, 6 (2018) Article No. 21. doi: 10.3389/fchem.2018.00021
 7. W. Li, H. Li, Z. Lu, L. Gan, L. Ke, T. Zhai, and H. Zhou, *Energy Environ. Sci.*, 8 (2015) 3629
 8. Y. Liu, X. Xiao, X. Fan, M. Li, Y. Zhang, W. Zhang, and L. Chen, *J. Alloys Compd.*, 744 (2018) 15.
 9. W. Li, L. Ke, Y. Wei, S. Guo, L. Gan, H. Li, T. Zhai, and H. Zhou, *J. Mater. Chem. A*, 5 (2017) 4413.
 10. S. Haghghat-Shishavan, M. Nazarian-Samani, M. Nazarian-Samani, H.-K. Roh, K.-Y. Chung, S.-H. Oh, B.-W. Cho, S.F. Kashani-Bozorg, and K.-B. Kim, *ACS Appl. Mater. Interfaces*, 11 (2019) 32815.
 11. H. Shen, Z. Ma, B. Yang, B. Guo, Y. Lyu, P. Wang, H. Yang, Q. Li, H. Wang, Z. Liu, and A. Nie, *J. Power Sources*, 433 (2019) Article No. 126682. <https://doi.org/10.1016/j.jpowsour.2019.05.088>
 12. X. Li, W. Li, P. Shen, L. Yang, Y. Li, Z. Shi, H. Zhang, *Ceram. Int.*, 45 (2019) 15711.
 13. T. Wang, K. Zhang, M. Park, V.W. Lau, H. Wang, J. Zhang, J. Zhang, R. Zhao, Y. Yamauchi, and Y.-M. Kang, *ACS Nano*, 14 (2020) 4352.
 14. K.-H. Nam, K.-J. Jeon, C.-M. Park, *Energy Storage Materials*, 17 (2019) 78.
 15. K.-W. Tseng, S.-B. Huang, W.-C. Chang, and H.-Y. Tuan, *Chem. Mater.*, 30 (2018) 4440.
 16. T. Zeng, H. He, H. Guan, R. Yuan, X. Liu, and C. Zhang, *Angew. Chem. Int. Ed.*, 60 (2021) 12103.
 17. F. Yang, J. Hong, J. Hao, S. Zhang, G. Liang, J. Long, Y. Liu, N. Liu, W.K. Pang, J. Chen, and Z. Guo, *Adv. Energy Mater.*, 10 (2020) Iss. 14. Article No. 1903826. <https://doi.org/10.1002/aenm.201903826>.
 18. I.M. Gavrilin, V.A. Smolyaninov, A.A. Dronov, S.A. Gavrilov, A.Yu. Trifonov, T.L. Kulova, A.A. Kuz'mina, and A.M. Skundin, *Mendeleev Commun.*, 28 (2018) 659.
 19. I.M. Gavrilin, Yu.O. Kudryashova, A.A. Kuz'mina, T.L. Kulova, A.M. Skundin, V.V. Emets, R.L. Volkov, A.A. Dronov, N.I. Borgardt, S.A. Gavrilov, *J. Electroanalyt. Chem.*, 888 (2021) Article No. 115209. <https://doi.org/10.1016/j.jelechem.2021.115209>
 20. P. L. Stanghellini, E. Boccaleri, E. Diana, G. Alberti, and R. Vivani, *Inorg. Chem.*, 43(2004) 5698.
 21. J.E.B. Randles, *Trans. Faraday Soc.*, 44 (1948) 327.
 22. A. Ševčík, *Coll. Czechoslov. Chem. Comm.*, 13 (1948) 349.
 23. W. Peukert, *Elektrotechn. Zeitschr.*, 18 (1897) 287.
 24. A. Skundin, D. Gryzlov, T. Kulova, Y. Kudryashova, A. Kuz'mina, *Int. J. Electrochem. Sci.*, 15 (2020) 1622.